Available online at www.sciencedirect.com

ScienceDirect

International Journal of Solids and Structures 45 (2008) 303–319

INTERNATIONAL JOURNAL OF SOLIDS AND STRUCTURES

www.elsevier.com/locate/ijsolstr

Torsion of cylindrically orthotropic elastic circular bars with radial inhomogeneity: some exact solutions and end effects

Jiann-Quo Tarn *, Hsi-Hung Chang

Department of Civil Engineering, National Cheng Kung University, Tainan 70101, Taiwan, ROC

Received 28 December 2006; received in revised form 8 June 2007
Available online 1 September 2007

Abstract

Torsion of elastic circular bars of radially inhomogeneous, cylindrically orthotropic materials is studied with emphasis on the end effects. To examine the conjecture of Saint-Venant's torsion, we consider torsion of circular bars with one end fixed and the other end free on which tractions that results in a pure torque are prescribed arbitrarily over the free end surface. Exact solutions that satisfy the prescribed boundary conditions point by point over the entire boundary surfaces are derived in a unified manner for cylindrically orthotropic bars with or without radial inhomogeneity and for their counterparts of Saint-Venant's torsion. Stress diffusion due to the end effect is examined in the light of the exact solutions.

Keywords: Cylindrical orthotropy; End effect; Exact solutions; Radial inhomogeneity; Torsion

1. Introduction

Saint-Venant's torsion of a homogeneous, isotropic elastic circular bar is a classical problem of elasticity (Sokolnikoff, 1956), which was solved using the semi-inverse method by assuming a state of pure shear in the body such that it gives rise to a resultant torque over the end section. Extension to more complicated cases of anisotropic or non-homogeneous materials or both has been considered by Lekhnitskii (1981), Rooney and Ferrari (1995), Horgan and Chan (1999), Ting (1999), Tarn (2001, 2002a), Tarn and Wang (2001), Tarn and Chang (2005) and Chen and Wei (2005), among others. In particular, Dong and his coworkers (Dong et al., 2001; Huang and Dong, 2001; Kosmatka et al., 2001; Lin et al., 2001) used a semi-analytic finite element method to investigate the Saint-Venant problem of inhomogeneous, generally anisotropic cylinders with non-circular sections. A common feature of Saint-Venant's solutions for this class of problems is that the exact boundary conditions (BC) prescribed on the end surfaces are relaxed by considering the stress resultants over the end section. As such, for the solutions to be exact the end conditions cannot be arbitrarily prescribed – it must be specified in the same way as demanded by the theory – otherwise the stress

* Corresponding author. Fax: +886 6 2358542.
E-mail address: jqtarn@mail.ncku.edu.tw (J.-Q. Tarn).

0020-7683/$ - see front matter
doi:10.1016/j.ijsolstr.2007.08.012

field will be disturbed by the end effect. Questions arise as to how significant the end effect is: Is the disturbance confined to a local region? Will it be felt away from the end? More specifically, to what extent is the Saint-Venant solution applicable in case the exact BC is relaxed by a statically equivalent one? By virtue of Saint-Venant's principle, it is generally expected that the stress disturbance decays rapidly in a homogeneous, isotropic bar so that the solution can be used to evaluate the stress distribution in a long circular bar in the region away from the ends. When the bar is anisotropic, inhomogeneous, or of a finite length, the conjecture of Saint-Venant's torsion needs to be examined (Horgan, 1989, 1996), especially when there involve displacement BC such as the fixed end BC of a cantilever bar, which cannot be replaced by a statically equivalent one. In this regard, Folkes and Arridge (1975) in their measurement of shear modulus in highly anisotropic materials has reported that Saint-Venant's principle is not applicable to materials possessing a large mechanical anisotropy due to the slow decay of the non-uniform stress at the sample ends arising from the clamping method.

The slow decay of the end effects due to anisotropy was first pointed out in Horgan (1972). Subsequently, Horgan and his associates investigated the Saint-Venant end effects in a series of papers (Horgan, 1982; Horgan and Simmonds, 1994; Horgan and Miller, 1995; Scalpato and Horgan, 1997; Horgan and Chan, 1999). A comprehensive review of the relevant studies was given in a book chapter by Horgan and Carlsson (2000). While the decay behaviors were examined extensively, the exact deformation and stress disturbances due to the end effects were scarcely analyzed in the past. In this paper, we address the issues of the end effect through an exact analysis of the deformations and stress fields in finite circular bars under torsion. The material is assumed to be cylindrically orthotropic and radially inhomogeneous with functionally graded materials (FGM) in view. Cylindrical orthotropy and radial inhomogeneity exist in man-made and natural materials, for examples, in bamboo, tree trunk, and carbon fiber (Christensen, 1994). The metallic forming process of extrusion or drawing often results in cylindrical orthotropic products. To examine the conjecture of Saint-Venant's torsion, we consider torsion of circular bars with one end fixed and the other end free on which tractions that gives rise to a pure torque are prescribed over the free end surface. The problem is relevant to many physical situations, for instance, drive shafts that transmit power from one point to another, in which one end of the shaft is restrained and the other end is subjected to traction applied in a different manner from that assumed by Saint-Venant's torsion in practice.

The problem under study is formulated on the basis of the state space formalism for anisotropic elasticity (Tarn, 2002b). In the state space setting it becomes clear that the equations for axisymmetric problems of cylindrically orthotropic bodies (or bodies with higher elastic symmetry, such as transverse isotropy and isotropy) are uncoupled into two sets of equations: one for torsional deformation, another for extensional deformation. The uncoupling makes it possible for us to obtain the exact solutions for torsion of cylindrically othotropic circular bars without using the semi-inverse method. The exact solutions obtained herein satisfy the prescribed BC point by point over the entire boundary surfaces. Radially inhomogeneous FGM circular bars can be treated within the context as well. Exact solutions for cantilever circular bars with the power-law radial inhomogeneity and for Saint-Venant's torsion of circular bars with arbitrary radial inhomogeneity are derived in a unified manner.

The paper is arranged in the following order. First, the problem of torsion of cylindrically anisotropic circular bars is formulated in the state space setting. Next, solutions for Saint-Venant's torsion of cylindrically orthotropic circular bars with arbitrary radial inhomogeneity are determined within the context so as to provide a comparison basis for evaluating the end effect. Subsequently, exact solutions for torsion of cylindrically orthotropic cantilever circular bars are derived, followed by exact solutions for torsion of FGM cantilever circular bars with power-law radial inhomogeneity. Finally, the conjecture of Saint-Venant's torsion and the end effect are examined in the light of the exact solutions.

2. State space formulation

Consider torsion of circular bars with one end fixed and the other free on which the traction that results in a pure torque is prescribed over the end surface. Referred to cylindrical coordinates (r, θ, z), the medium is cylindrically orthotropic and radially inhomogeneous. The constitutive equations of the material are

$$\begin{bmatrix}\sigma_r\\ \sigma_\theta\\ \sigma_z\\ \sigma_{\theta z}\\ \sigma_{rz}\\ \sigma_{r\theta}\end{bmatrix}=\begin{bmatrix}c_{11} & c_{12} & c_{13} & 0 & 0 & 0\\ c_{12} & c_{22} & c_{23} & 0 & 0 & 0\\ c_{13} & c_{23} & c_{33} & 0 & 0 & 0\\ 0 & 0 & 0 & c_{44} & 0 & 0\\ 0 & 0 & 0 & 0 & c_{55} & 0\\ 0 & 0 & 0 & 0 & 0 & c_{66}\end{bmatrix}\begin{bmatrix}\varepsilon_r\\ \varepsilon_\theta\\ \varepsilon_z\\ 2\varepsilon_{\theta z}\\ 2\varepsilon_{rz}\\ 2\varepsilon_{r\theta}\end{bmatrix}, \tag{1}$$

where $\varepsilon_r, \varepsilon_\theta, \ldots; \sigma_r, \sigma_\theta, \ldots$ are the strain and stress components, c_{ij} are the nine independent elastic constants of the cylindrically orthotropic material, which are dependent on the radial coordinate, $c_{ij} = c_{ij}(r)$, for radially inhomogeneous materials.

The strain–displacement relations for axisymmetric deformations are

$$\varepsilon_r = u_{r,r}, \quad \varepsilon_\theta = r^{-1}u_r, \quad \varepsilon_z = u_{z,z},$$
$$2\varepsilon_{\theta z} = u_{\theta,z}, \quad 2\varepsilon_{rz} = u_{z,r} + u_{r,z}, \quad 2\varepsilon_{r\theta} = u_{\theta,r} - r^{-1}u_\theta, \tag{2}$$

where a comma stands for differentiation with respect to the suffix variables.

The equilibrium equations in the absence of the body force are

$$\partial_r\sigma_r + r^{-1}(\sigma_r - \sigma_\theta) + \partial_z\sigma_{rz} = 0, \tag{3}$$
$$\partial_r\sigma_{r\theta} + 2r^{-1}\sigma_{r\theta} + \partial_z\sigma_{\theta z} = 0, \tag{4}$$
$$\partial_r\sigma_{rz} + r^{-1}\sigma_{rz} + \partial_z\sigma_z = 0, \tag{5}$$

where ∂_r and ∂_z denote partial differentiation with respect to r and z, respectively.

On the basis of the state space formalism of anisotropic elasticity in the cylindrical coordinate system (Tarn, 2002b), Eqs. (1)–(5) can be formulated into two uncoupled sets of matrix equations in the state space setting as follows:

$$\frac{\partial}{\partial z}\begin{bmatrix}u_r\\ u_z\\ \sigma_{rz}\\ \sigma_{zz}\end{bmatrix}=\begin{bmatrix}0 & -\partial_r & c_{55}^{-1} & 0\\ d_{21} & 0 & 0 & c_{33}^{-1}\\ d_{31} & 0 & 0 & d_{34}\\ 0 & 0 & -\partial_r - r^{-1} & 0\end{bmatrix}\begin{bmatrix}u_r\\ u_z\\ \sigma_{rz}\\ \sigma_{zz}\end{bmatrix}, \tag{6}$$

$$\begin{bmatrix}\sigma_{rr}\\ \sigma_{\theta\theta}\end{bmatrix}=\begin{bmatrix}\tilde{c}_{11}\partial_r + r^{-1}\tilde{c}_{12} & \hat{c}_{13}\\ \tilde{c}_{12}\partial_r + r^{-1}\tilde{c}_{22} & \hat{c}_{23}\end{bmatrix}\begin{bmatrix}u_r\\ \sigma_{zz}\end{bmatrix}, \tag{7}$$

and

$$\frac{\partial}{\partial z}\begin{bmatrix}u_\theta\\ \sigma_{\theta z}\end{bmatrix}=\begin{bmatrix}0 & c_{44}^{-1}\\ -r^{-1}[(\partial_r + r^{-1})rc_{66}(\partial_r - r^{-1})] & 0\end{bmatrix}\begin{bmatrix}u_\theta\\ \sigma_{\theta z}\end{bmatrix}, \tag{8}$$
$$\sigma_{r\theta} = c_{66}(\partial_r - r^{-1})u_\theta, \tag{9}$$

where

$$\hat{c}_{ij} = c_{ij}c_{33}^{-1}, \quad \tilde{c}_{ij} = c_{ij} - c_{i3}c_{33}^{-1}c_{j3}, \quad d_{21} = -\hat{c}_{13}\partial_r - r^{-1}\hat{c}_{23},$$
$$d_{31} = -r^{-1}[\partial_r(\tilde{c}_{11}r\partial_r) + \partial_r\tilde{c}_{12} - \tilde{c}_{12}\partial_r - r^{-1}\tilde{c}_{22}], \quad d_{34} = -r^{-1}[\partial_r(r\hat{c}_{13}) - \hat{c}_{23}].$$

Solution of the state equations, Eqs. (6) and (8), must be supplemented with BC. For torsion problems of circular bars with one end fixed and the other free on which the traction that results in a pure torque is prescribed over the end surface, the BC at the fixed end $z = 0$ and at the free end $z = l$ are

$$u_r = u_z = 0, \quad u_\theta = 0 \ \text{ at } z = 0, \tag{10}$$
$$\sigma_{rz} = \sigma_{zz} = 0, \quad \sigma_{\theta z} = p(r) \ \text{ at } z = l, \tag{11}$$

where the prescribed traction p is a function of r, which produces a pure torque M_t such that

$$\int_0^{2\pi}\int_0^b pr^2\,\mathrm{d}r\,\mathrm{d}\theta = M_\mathrm{t}. \tag{12}$$

The traction-free BC on the cylindrical surface are

$$\sigma_{rr} = \sigma_{rz} = 0, \quad \sigma_{r\theta} = 0 \ \text{ at } r = b, \tag{13}$$

where b is the radius of the circular bar.

Eqs. (6)–(9) and the associated BC suggest that the torsional deformation is not coupled with extensional deformation in a cylindrically orthotropic circular cylinder. Before proceeding to deriving the exact solutions for cantilever circular bars, we shall revisit Saint-Venant's torsion and derive the solution for the problem in the present context so as to provide a comparison basis in quantification of the end effect.

3. Saint-Venant's torsion

For Saint-Venant's torsion of circular bars the exact end conditions given by Eqs. (10) and (11) are relaxed by considering the stress resultants such that the traction components over the end sections produce a pure torque. The statically equivalent end conditions in full are

$$\int_0^{2\pi}\int_0^b [\,\sigma_{zz}r\sin\theta \quad \sigma_{zz}r\cos\theta \quad \sigma_{\theta z}r\,]r\mathrm{d}r\,\mathrm{d}\theta = [\,0 \quad 0 \quad M_\mathrm{t}\,], \tag{14}$$

$$\int_0^{2\pi}\int_0^b [\,\sigma_{rz}\cos\theta - \sigma_{\theta z}\sin\theta \quad \sigma_{rz}\sin\theta + \sigma_{\theta z}\cos\theta \quad \sigma_{zz}\,]r\mathrm{d}r\,\mathrm{d}\theta = \mathbf{0}. \tag{15}$$

Without recourse to the semi-inverse method with a priori assumptions, it can be shown that indeed the solution for Eq. (6) together with Eq. (13a), Eqs. (14a,b), and Eq. (15) is trivial,

$$u_r = u_z = \sigma_{rz} = \sigma_{zz} = \sigma_{rr} = \sigma_{\theta\theta} = 0. \tag{16}$$

Now, the task of determining the solution for Saint-Venant's torsion is to solve Eq. (8) subjected to the remaining BC:

$$\sigma_{r\theta} = 0 \quad \text{at } r = b, \tag{17}$$

$$\int_0^{2\pi}\int_0^b \sigma_{\theta z}r^2\mathrm{d}r\,\mathrm{d}\theta = M_\mathrm{t}. \tag{18}$$

3.1. Homogeneous bars

By using separation of variables, we seek the solution to Eq. (8) of the form

$$\begin{bmatrix} u_\theta \\ \sigma_{\theta z} \end{bmatrix} = f(r)\begin{bmatrix} U(z) \\ S(z) \end{bmatrix}, \tag{19}$$

so that Eq. (8) is separated into

$$\frac{\mathrm{d}}{\mathrm{d}z}\begin{bmatrix} U \\ S \end{bmatrix} = \begin{bmatrix} 0 & c_{44}^{-1} \\ \lambda^2 c_{66} & 0 \end{bmatrix}\begin{bmatrix} U \\ S \end{bmatrix}, \tag{20}$$

$$\left(\frac{\mathrm{d}^2}{\mathrm{d}r^2} + \frac{1}{r}\frac{\mathrm{d}}{\mathrm{d}r} - \frac{1}{r^2}\right)f(r) = \lambda^2 f(r), \tag{21}$$

where λ is a constant parameter which may be zero, real or imaginary. For Saint-Venant's torsion it suffices to take $\lambda = 0$ to determine the solution.

The solutions of Eqs. (20) and (21) for $\lambda = 0$ are

$$\begin{bmatrix} U(z) \\ S(z) \end{bmatrix} = \begin{bmatrix} c_0' + z \\ c_{44} \end{bmatrix}, \tag{22}$$

$$f(r) = c_1 r + c_2 r^{-1}, \tag{23}$$

where c_0', c_1 and c_2 are undetermined constants.

To avoid displacement and stress being unbounded at $r = 0$, we must set $c_2 = 0$. Further, the constant $c_0 = 0$ so as to satisfy the fixed end BC at $z = 0$. There follows

$$\begin{bmatrix} u_\theta \\ \sigma_{\theta z} \end{bmatrix} = c_1 \begin{bmatrix} rz \\ c_{44} r \end{bmatrix}, \quad \sigma_{r\theta} = 0, \tag{24}$$

where c_1 is a constant to be determined. The equation satisfies the BC on the cylindrical surface $r = b$ identically.

Upon substituting Eq. (24) in Eq. (18) to determine c_1, we obtain

$$u_\theta = \frac{M_t}{D} rz, \quad \sigma_{\theta z} = c_{44} \frac{M_t}{D} r, \quad \sigma_{r\theta} = 0, \quad D = \frac{\pi c_{44}}{2} b^4, \tag{25}$$

in which D is the torsional rigidity.

The result agrees with that in Lekhnitskii (1981) using the stress function approach. It is interesting to note that Eq. (25) satisfies the fixed end BC at $z = 0$ identically without handling it in particular. Hence the solution holds for a cantilever bar provided that the exact traction BC at the free end is replaced by the condition requiring the stress resultant equal to M_t.

3.2. Radially inhomogeneous bars

Consider Saint-Venant's torsion of a FGM circular bar with material properties varying in the radial direction such that the elastic constants $c_{ij} = c_{ij}(r)$ are arbitrary, differentiable functions of r. We seek the solution to Eq. (8) by separation of variables.

Let

$$\begin{bmatrix} u_\theta \\ \sigma_{\theta z} \end{bmatrix} = f(r) \begin{bmatrix} U(z) \\ S(z) \end{bmatrix}. \tag{26}$$

Eq. (8) is then separated into

$$\frac{\mathrm{d}}{\mathrm{d}z} \begin{bmatrix} U \\ S \end{bmatrix} = \begin{bmatrix} 0 & c_{44}^{-1} \\ \lambda^2 & 0 \end{bmatrix} \begin{bmatrix} U \\ S \end{bmatrix}, \tag{27}$$

and

$$-\frac{1}{r}\left[\left(\frac{\mathrm{d}}{\mathrm{d}r} + \frac{1}{r}\right) r c_{66}(r) \left(\frac{\mathrm{d}}{\mathrm{d}r} - \frac{1}{r}\right)\right] f(r) = \lambda^2 f(r), \tag{28}$$

to which the solution depends on the parameter λ. For this problem it suffices to take $\lambda = 0$ to determine the solution.

The solutions of Eqs. (27) and (28) for $\lambda = 0$ are

$$\begin{bmatrix} U(z) \\ S(z) \end{bmatrix} = \begin{bmatrix} c_0' + z \\ c_{44} \end{bmatrix}, \tag{29}$$

$$f(r) = c_1 r + c_2 r \int \frac{\mathrm{d}r}{r^3 c_{66}(r)}. \tag{30}$$

There follows

$$\begin{bmatrix} u_\theta \\ \sigma_{\theta z} \end{bmatrix} = \begin{bmatrix} c_1 rz + c_2 h(r) z + c_3 h(r) + c_0 r \\ c_{44}(r)[c_1 r + c_2 h(r)] \end{bmatrix}, \tag{31}$$

$$\sigma_{r\theta} = r^{-2}(c_2 z + c_3), \tag{32}$$

where $h(r)$ is defined by

$$h(r) \equiv r \int \frac{\mathrm{d}r}{r^3 c_{66}(r)}.$$

Upon setting $c_0 = c_2 = c_3 = 0$ to avoid unbounded stress at $r = 0$ and to satisfy the fixed end BC at $z = 0$, and substituting Eq. (31b) into Eq. (18) to determine c_1, we obtain

$$u_\theta = \frac{M_\mathrm{t}}{D} rz, \quad \sigma_{\theta z} = c_{44}(r)\frac{M_\mathrm{t}}{D} r, \quad \sigma_{r\theta} = 0, \quad D = 2\pi \int_0^b r^3 c_{44}(r)\mathrm{d}r, \tag{33}$$

which is essentially the same as Eq. (25) for a homogeneous circular bar apart from the torsional rigidity D. Eq. (25) is recovered by letting $c_{44}(r)$ be independent of r.

The solution satisfies the fixed end BC at $z = 0$ identically, in which only the exact traction BC at the free end has been relaxed by a statically equivalent one. Note that among various elastic constants only $c_{44}(r) \equiv G_\mathrm{L}(r)$ enters the stage, G_L being the longitudinal shear modulus of the cylindrically orthotropic material.

As an example, consider a FGM circular bar with power-law radial inhomogeneity such that $c_{44}(r) = a_{44}(r/b)^{2\mu}$, where the coefficient a_{44} has the same dimension as the elastic constant c_{44}, μ is a non-negative real number. There follows

$$u_\theta = \frac{(\mu+2)M_\mathrm{t}}{\pi b^4 a_{44}} rz, \quad \sigma_{\theta z} = \frac{(\mu+2)M_\mathrm{t}}{\pi b^{2(\mu+2)}} r^{2\mu+1}, \quad \sigma_{r\theta} = 0, \tag{34}$$

which is useful in evaluating the end effects in circular bars with radial inhomogeneity.

4. Exact solutions for torsion of finite bars

4.1. Homogeneous bars

We now derive the exact solutions for torsion of cantilever circular bars. Eqs. (6) and (7) and the associated BC are identically satisfied by letting

$$u_r = u_z = \sigma_{rz} = \sigma_{zz} = \sigma_{rr} = \sigma_{\theta\theta} = 0. \tag{35}$$

It remains to solve Eq. (8) subjected to

$$\sigma_{r\theta} = 0 \quad \text{at } r = b, \tag{36}$$

$$u_\theta = 0 \quad \text{at } z = 0, \tag{37}$$

$$\sigma_{\theta z} = p(r) \quad \text{at } z = l, \tag{38}$$

in which p is an arbitrary function of r, which gives rise to pure torque at the free end.

We seek the solution to Eq. (8) of the form

$$\begin{bmatrix} u_\theta \\ \sigma_{\theta z} \end{bmatrix} = f(r)\begin{bmatrix} U(z) \\ S(z) \end{bmatrix}. \tag{39}$$

Eq. (8) is then separated into

$$\frac{\mathrm{d}}{\mathrm{d}z}\begin{bmatrix} U \\ S \end{bmatrix} = \begin{bmatrix} 0 & c_{44}^{-1} \\ \lambda^2 c_{66} & 0 \end{bmatrix}\begin{bmatrix} U \\ S \end{bmatrix}, \tag{40}$$

$$\left(\frac{\mathrm{d}^2}{\mathrm{d}r^2} + \frac{1}{r}\frac{\mathrm{d}}{\mathrm{d}r} - \frac{1}{r^2}\right) f(r) = -\lambda^2 f(r), \tag{41}$$

to which the solutions depend on the eigenvalue λ. For the problem of a finite circular bar it is necessary to include the solution associated with $\lambda \neq 0$, in addition to Eqs. (22) and (23) for $\lambda = 0$.

For $\lambda \neq 0$, the solutions of Eqs. (40) and (41) are

$$\begin{bmatrix} U \\ S \end{bmatrix} = \begin{bmatrix} \exp(\kappa\lambda z) & \exp(-\kappa\lambda z) \\ \kappa\lambda c_{44}\exp(\kappa\lambda z) & -\kappa\lambda c_{44}\exp(-\kappa\lambda z) \end{bmatrix} \begin{bmatrix} d_1 \\ d_2 \end{bmatrix}, \quad \kappa = \sqrt{\frac{c_{66}}{c_{44}}}, \tag{42}$$

$$f(r) = d_3 J_1(\lambda r) + d_4 Y_1(\lambda r), \tag{43}$$

in which d_k are undetermined constants, $J_1(\lambda r)$ and $Y_1(\lambda r)$ are Bessel functions of the first kind and the second kind, of order *1*, respectively.

The constants c_2 in Eq. (23) and d_4 in Eq. (43) must be set to zero so as to avoid unbounded displacement and unbounded stress at $r = 0$. There follows

$$\begin{bmatrix} u_\theta \\ \sigma_{\theta z} \end{bmatrix} = \begin{bmatrix} c_0 r + c_1 r z \\ c_1 c_{44} r \end{bmatrix} + J_1(\lambda r) \begin{bmatrix} \exp(\kappa\lambda z) & \exp(-\kappa\lambda z) \\ \kappa\lambda c_{44}\exp(\kappa\lambda z) & -\kappa\lambda c_{44}\exp(-\kappa\lambda z) \end{bmatrix} \begin{bmatrix} d_5 \\ d_6 \end{bmatrix}, \tag{44}$$

$$\sigma_{r\theta} = -c_{66}\lambda J_2(\lambda r)[\exp(\kappa\lambda z) \quad \exp(-\kappa\lambda z)] \begin{bmatrix} d_5 \\ d_6 \end{bmatrix}, \tag{45}$$

where we arrive at Eq. (45) by using the relation of the Bessel functions (Watson, 1995; Hildebrand, 1976):

$$\frac{\mathrm{d}}{\mathrm{d}x} y_\nu(\lambda x) - \frac{\nu}{x} y_\nu(\lambda x) = -\lambda y_{\nu+1}(\lambda x) \quad (y = J, Y) \tag{46}$$

Imposing on Eq. (45) the traction-free BC at $r = b$ yields

$$\lambda J_2(\lambda b) = 0, \tag{47}$$

thus, in addition to $\lambda_0 = 0$, the eigenvalues λ_n $(n = 1, 2, \ldots)$ are the zeros of $J_2(bx)$, which are real and positive.

A linear combination of the solutions associated with λ_n $(n = 0, 1, 2, \ldots)$ produces

$$u_\theta = c_0 r + c_1 r z + \sum_{n=1}^{\infty} [A_n \exp(\kappa\lambda_n z) + B_n \exp(-\kappa\lambda_n z)] J_1(\lambda_n r), \tag{48}$$

$$\sigma_{\theta z} = c_{44}\left[c_1 r + \kappa \sum_{n=1}^{\infty} \lambda_n [A_n \exp(\kappa\lambda_n z) - B_n \exp(-\kappa\lambda_n z)] J_1(\lambda_n r)\right], \tag{49}$$

$$\sigma_{r\theta} = -c_{66} \sum_{n=1}^{\infty} \lambda_n [A_n \exp(\kappa\lambda_n z) + B_n \exp(-\kappa\lambda_n z)] J_2(\lambda_n r). \tag{50}$$

Imposing the displacement BC at $z = 0$ on Eq. (48) and the traction BC at $z = l$ on Eq. (49) yields

$$c_0 r + \sum_{n=1}^{\infty} (A_n + B_n) J_1(\lambda_n r) = 0, \tag{51}$$

$$c_1 r + \kappa \sum_{n=1}^{\infty} [A_n \exp(\kappa\lambda_n l) - B_n \exp(-\kappa\lambda_n l)] \lambda_n J_1(\lambda_n r) = c_{44}^{-1} p(r), \tag{52}$$

to determine the constants c_0, c_1, A_n, and B_n in the solution.

It is easy to find from Eq. (51): $c_0 = 0$, $B_n = -A_n$, thus Eq. (52) becomes

$$c_1 r + 2\kappa \sum_{n=1}^{\infty} A_n \lambda_n \cosh(\kappa\lambda_n l) J_1(\lambda_n r) = c_{44}^{-1} p(r). \tag{53}$$

By using Dini's expansion (Watson, 1995, p. 597) to express $p(r)$ in the form of Fourier–Bessel series and comparing the coefficients on both sides, we find

$$c_1 = \frac{4}{c_{44}b^4}\int_0^b r^2 p(r)\mathrm{d}r = \frac{2M_\mathrm{t}}{c_{44}\pi b^4}, \tag{54}$$

$$A_n = \frac{1}{\kappa c_{44} b^2 \lambda_n \cosh(\kappa\lambda_n l) J_1^2(\lambda_n b)}\int_0^b rp(r)J_1(\lambda_n r)\mathrm{d}r. \tag{55}$$

As a result,

$$u_\theta = \frac{2M_\mathrm{t}}{c_{44}\pi b^4} rz + 2\sum_{n=1}^{\infty} A_n J_1(\lambda_n r)\sinh(\kappa\lambda_n z), \tag{56}$$

$$\sigma_{\theta z} = \frac{2M_\mathrm{t}}{\pi b^4} r + 2\kappa c_{44}\sum_{n=1}^{\infty} A_n\lambda_n J_1(\lambda_n r)\cosh(\kappa\lambda_n z), \tag{57}$$

$$\sigma_{r\theta} = -2c_{66}\sum_{n=1}^{\infty} A_n\lambda_n J_2(\lambda_n r)\sinh(\kappa\lambda_n z). \tag{58}$$

By inspection, we find that the leading terms in Eqs. (56)–(58) are precisely their Saint-Venant counterparts and the transverse shear stress $\sigma_{r\theta} \neq 0$ in contrast with $\sigma_{r\theta} = 0$ everywhere in Eq. (25). The series terms in the exact solution depend on the material parameter $\kappa = (c_{66}/c_{44})^{1/2} \equiv (G_\mathrm{T}/G_\mathrm{L})^{1/2}$, G_T and G_L being the transverse shear modulus and the longitudinal shear modulus, respectively, whereas the Saint-Venant solution depend only on $c_{44} \equiv G_\mathrm{L}$. The solution remains unchanged for circular bars of transversely isotropic materials. For isotropic materials $G_\mathrm{T} = G_\mathrm{L}$ so that $\kappa = 1$ in the solution.

Eqs. (56)–(58) tell us that the displacement and the stresses at $z = 0$ are

$$u_\theta = \sigma_{r\theta} = 0, \quad \sigma_{\theta z} = \frac{2M_\mathrm{t}}{\pi b^4} r + 2\kappa c_{44}\sum_{n=1}^{\infty} A_n\lambda_n J_1(\lambda_n r), \tag{59}$$

so that u_θ and $\sigma_{r\theta}$ vanish at the fixed end as in Saint-Venant's torsion, but the longitudinal shear stress $\sigma_{\theta z}$ is affected by the load distribution at the free end (through A_n) as well as the material anisotropy (through $\kappa c_{44} \equiv \sqrt{c_{44}c_{66}}$), in addition to the eigenvalues λ_n. We shall examine the end effect quantitatively later on.

As a simple check, let us specify the traction on the free end surface as $p(r) = kr$, in accordance with $\sigma_{\theta z}$ being a linear function of r according to Saint-Venant's torsion. Then, we obtain from Eq. (12), and (55):

$$k = \frac{2M_\mathrm{t}}{\pi b^4}, \quad A_n \sim k\int_0^b r^2 J_1(\lambda_n r)\mathrm{d}r = \frac{k}{\lambda_n} b^2 J_2(\lambda_n b) = 0, \tag{60}$$

in which $A_n = 0$ because of Eq. (47). It follows that the series terms in Eqs. (56)–(58) vanish and the solutions are preciously their Saint-Venant counterparts given by Eq. (25).

This confirms that the Saint-Venant solution is valid everywhere in the bar in case the traction over the end surface is specified as a linear function of r a posterior. If $p(r)$ is prescribed otherwise, $A_n \neq 0$ and k are not given by Eq. (60). As a result, stress disturbance due to the end effect occurs – both the leading terms and the series terms in Eqs. (56)–(58) render the Saint-Venant solution in error.

4.2. Radially inhomogeneous bars

We are now in a position to consider torsion of FGM cantilever circular bars with material properties varying in the radial direction such that the elastic constants $c_{ij} = c_{ij}(r)$ are arbitrary differentiable functions of r. By using the separation of variables, we seek the solution to Eq. (8) of the form

$$\begin{bmatrix} u_\theta \\ \sigma_{\theta z} \end{bmatrix} = f(r)\begin{bmatrix} U(z) \\ c_{44}S(z) \end{bmatrix}, \tag{61}$$

so that Eq. (8) is separated into

$$\frac{\mathrm{d}}{\mathrm{d}z}\begin{bmatrix} U \\ S \end{bmatrix} = \begin{bmatrix} 0 & 1 \\ \alpha^2 & 0 \end{bmatrix}\begin{bmatrix} U \\ S \end{bmatrix}, \tag{62}$$

$$-\frac{1}{r}\left[\left(\frac{\mathrm{d}}{\mathrm{d}r}+\frac{1}{r}\right)rc_{66}(r)\left(\frac{\mathrm{d}}{\mathrm{d}r}-\frac{1}{r}\right)\right]f(r) = \alpha^2 c_{44}(r)f(r), \tag{63}$$

where α is a constant which may be zero, real or imaginary.

For $\alpha \neq 0$, Eq. (63) with arbitrary $c_{44}(r)$ and $c_{66}(r)$ is unsolvable in a closed form. The only class of radial inhomogeneity that allows an exact solution of Eq. (63) seems to be that having variation defined by

$$c_{ij}(r) = a_{ij}(r/b)^{2\mu}, \tag{64}$$

where the coefficient a_{ij} have the same dimension as c_{ij}, μ is a non-negative real number. The homogeneous material is a special case with $\mu = 0$.

Such a radial inhomogeneity, known as the power-law radial inhomogeneity, was usually assumed in stress analysis of FGM in cylindrical coordinates (Lekhnitskii, 1981; Horgan and Chan, 1999; Yang, 2000; Tarn, 2001; among others). Although it is possible to obtain an approximate solution for arbitrary radial inhomogeneity by using piecewise-constant representation of the material properties in conjunction with the method of transfer matrix (Tarn and Chang, 2005), in keeping with the main theme of the present study, we confine ourselves to determining the exact solution for a cantilever circular bar with the power-law radial inhomogeneity.

Substituting Eq. (64) into Eq. (63) yields

$$r^2\frac{\mathrm{d}^2 f}{\mathrm{d}r^2} + (2\mu+1)r\frac{\mathrm{d}f}{\mathrm{d}r} + (\lambda^2 r^2 - 2\mu - 1)f = 0, \quad \kappa = \sqrt{\frac{a_{66}}{a_{44}}}, \quad \lambda = \frac{\alpha}{\kappa}, \tag{65}$$

which is a differential equation satisfied by Bessel functions (Hildebrand, 1976, p. 152) and the solution is

$$f(r) = r^{-\mu}[c_1 J_{\mu+1}(\lambda r) + c_2 Y_{\mu+1}(\lambda r)], \tag{66}$$

where $J_{\mu+1}(\lambda r)$ and $Y_{\mu+1}(\lambda r)$ are Bessel functions of the first kind and the second kind, of order $\mu+1$, respectively. The solution of Eq. (62) for $\lambda \neq 0$ is

$$\begin{bmatrix} U \\ S \end{bmatrix} = \begin{bmatrix} \exp(\kappa\lambda z) & \exp(-\kappa\lambda z) \\ \kappa\lambda\exp(\kappa\lambda z) & -\kappa\lambda\exp(-\kappa\lambda z) \end{bmatrix}\begin{bmatrix} c_3 \\ c_4 \end{bmatrix}. \tag{67}$$

There follows

$$u_\theta = r^{-\mu}[c_1 J_{\mu+1}(\lambda r) + c_2 Y_{\mu+1}(\lambda r)][c_3\exp(\kappa\lambda z) + c_4\exp(-\kappa\lambda z)], \tag{68}$$

$$\sigma_{\theta z} = a_{44}\kappa\lambda b^{-2\mu}r^{\mu}[c_1 J_{\mu+1}(\lambda r) + c_2 Y_{\mu+1}(\lambda r)][c_3\exp(\kappa\lambda z) - c_4\exp(-\kappa\lambda z)], \tag{69}$$

$$\sigma_{r\theta} = -a_{66}\lambda b^{-2\mu}r^{\mu}[c_1 J_{\mu+2}(\lambda r) + c_2 Y_{\mu+2}(\lambda r)][c_3\exp(\kappa\lambda z) + c_4\exp(-\kappa\lambda z)], \tag{70}$$

where we have used Eq. (46) to arrive at Eq. (70).

The solutions of Eq. (62) and (65) for $\lambda = 0$ are

$$\begin{bmatrix} U(z) \\ S(z) \end{bmatrix} = \begin{bmatrix} c_0' z + c_1' \\ c_0' \end{bmatrix}, \tag{71}$$

$$f(r) = c_2' r + c_3' r^{-(2\mu+1)}. \tag{72}$$

Thus

$$u_\theta = d_0 r + d_1 r z + d_2 r^{-(2\mu+1)}z + d_3 r^{-(2\mu+1)}, \tag{73}$$

$$\sigma_{\theta z} = a_{44}b^{-2\mu}(d_1 r^{2\mu+1} + d_2 r^{-1}), \tag{74}$$

$$\sigma_{r\theta} = -2(\mu+1)a_{66}b^{-2\mu}r^{-2}(d_2 z + d_3). \tag{75}$$

Upon setting $c_2 = d_2 = d_3 = 0$ in these expressions so as to drop the terms of negative powers of r and the terms of $Y_{\mu+1}(\lambda r)$ and $Y_{\mu+2}(\lambda r)$ which are unbounded at $r = 0$, and imposing on $\sigma_{r\theta}$ the traction-free BC at $r = b$, we obtain

$$\lambda J_{\mu+2}(\lambda b) = 0, \tag{76}$$

hence, in addition to $\lambda_0 = 0$, the eigenvalues λ_n $(n = 1, 2, \ldots)$ are the zeros of $J_{\mu+2}(\lambda b)$, which are real and positive. A linear combination of the solutions associated with λ_n $(n = 0, 1, 2, \ldots)$ produces

$$u_\theta = d_0 r + d_1 r z + r^{-\mu} \sum_{n=1}^{\infty} [A_n \exp(\kappa\lambda_n z) + B_n \exp(-\kappa\lambda_n z)] J_{\mu+1}(\lambda_n r), \tag{77}$$

$$\sigma_{\theta z} = a_{44} b^{-2\mu} \left[d_1 r^{2\mu+1} + \kappa r^{\mu} \sum_{n=1}^{\infty} \lambda_n [A_n \exp(\kappa\lambda_n z) - B_n \exp(-\kappa\lambda_n z)] J_{\mu+1}(\lambda_n r) \right], \tag{78}$$

$$\sigma_{r\theta} = -a_{66} b^{-2\mu} r^{\mu} \sum_{n=1}^{\infty} \lambda_n [A_n \exp(\kappa\lambda_n z) + B_n \exp(-\kappa\lambda_n z)] J_{\mu+2}(\lambda_n r). \tag{79}$$

Imposing the displacement BC at $z = 0$ on Eq. (77) and the traction BC at $z = l$ on Eq. (78) gives

$$d_0 r^{\mu+1} + \sum_{n=1}^{\infty} (A_n + B_n) J_{\mu+1}(\lambda_n r) = 0, \tag{80}$$

$$d_1 r^{2\mu+1} + \kappa r^{\mu} \sum_{n=1}^{\infty} \lambda_n [A_n \exp(\kappa\lambda_n l) - B_n \exp(-\kappa\lambda_n l)] J_{\mu+1}(\lambda_n r) = a_{44}^{-1} b^{2\mu} p(r), \tag{81}$$

from Eq. (80), $d_0 = 0$, $B_n = -A_n$, then Eq. (81) becomes

$$d_1 r^{\mu+1} + 2\kappa \sum_{n=1}^{\infty} A_n \lambda_n \cosh(\kappa\lambda_n l) J_{\mu+1}(\lambda_n r) = a_{44}^{-1} b^{2\mu} r^{-\mu} p(r). \tag{82}$$

The left-hand side of Eq. (82) takes the form of Fourier–Bessel series. By using Dini's expansion (Watson, 1995) to express $r^{-\mu} p(r)$ in Fourier–Bessel series and comparing the coefficients on both sides, we obtain

$$d_1 = \frac{2(\mu+2)}{a_{44} b^4} \int_0^b r^2 p(r) \mathrm{d}r = \frac{(\mu+2) M_t}{a_{44} \pi b^4}, \tag{83}$$

$$A_n = \frac{1}{\kappa a_{44} b^{2(1-\mu)} \lambda_n \cosh(\kappa\lambda_n l) J_{\mu+1}^2(\lambda_n b)} \int_0^b r^{1-\mu} p(r) J_{\mu+1}(\lambda_n r) \mathrm{d}r. \tag{84}$$

As a result,

$$u_\theta = \frac{(\mu+2) M_t}{a_{44} \pi b^4} r z + 2 r^{-\mu} \sum_{n=1}^{\infty} A_n J_{\mu+1}(\lambda_n r) \sinh(\kappa\lambda_n z), \tag{85}$$

$$\sigma_{\theta z} = \frac{(\mu+2) M_t}{\pi b^{2(\mu+2)}} r^{2\mu+1} + 2\kappa a_{44} \frac{r^{\mu}}{b^{2\mu}} \sum_{n=1}^{\infty} \lambda_n A_n J_{\mu+1}(\lambda_n r) \cosh(\kappa\lambda_n z), \tag{86}$$

$$\sigma_{r\theta} = -2 a_{66} \frac{r^{\mu}}{b^{2\mu}} \sum_{n=1}^{\infty} \lambda_n A_n J_{\mu+2}(\lambda_n r) \sinh(\kappa\lambda_n z). \tag{87}$$

which reduces to Eqs. (56)–(58) for a homogeneous circular bar by letting $\mu = 0$.

At the fixed end $z = 0$,

$$u_\theta = \sigma_{r\theta} = 0, \quad \sigma_{\theta z} = \frac{(\mu+2) M_t}{\pi b^{2(\mu+2)}} r^{2\mu+1} + 2\kappa a_{44} \frac{r^{\mu}}{b^{2\mu}} \sum_{n=1}^{\infty} \lambda_n A_n J_{\mu+1}(\lambda_n r), \tag{88}$$

which indicates that the displacement and the transverse shear stress vanish at the fixed end as in Saint-Venant's torsion, but the longitudinal shear stress $\sigma_{\theta z}$ is affected by the load distribution at the free end, the material anisotropy and the radial inhomogeneity, in addition to the eigenvalues λ_n.

Suppose that the traction on the free end surface is prescribed as $p(r) = kr^{2\mu+1}$, in accordance with the radial distribution of $\sigma_{\theta z}$ given by Eq. (34) for Saint-Venant's torsion, there follows from Eq. (12), Eqs. (83), (84), and (76):

$$k = \frac{(\mu+2)M_t}{\pi b^{2(\mu+2)}}, \quad A_n \sim k\int_0^b r^{\mu+2}J_{\mu+1}(\lambda_n r)\mathrm{d}r = \frac{kb^{\mu+2}}{\lambda_n}J_{\mu+2}(\lambda_n b) = 0, \tag{89}$$

so that the series terms in Eqs. (85)–(87) vanish and the solutions are precisely the same as their Saint-Venant counterparts given by Eq. (34).

The results show that the Saint-Venant solution is exact provided that the traction over the end surface is prescribed in a particular manner as assumed above. In practice, one can hardly apply $p(r)$ in the same manner as demanded. Consequently, stress disturbance due to the end effect occurs. In the next section we shall evaluate the end effect quantitatively by comparing Eq. (34) for Saint-Venant's torsion against the exact solution given by Eqs. (85)–(87).

5. Results and discussion

It has been shown that the leading terms in the exact solution are identical to the Saint-Venant solution and the end effects are described solely by the series terms of Eqs. (56)–(58). Obviously, the BC at both ends of a finite circular bar play important roles in the stress distribution and they are indistinguishable in general. Yet, for a sufficiently long bar it can be deduced from Eqs. (48)–(50) and (77)–(79) that the stress diffusion from the end is essentially dictated by the terms associated with $\exp(-\kappa\lambda_n z)$ since the terms of $\exp(\kappa\lambda_n z)$ which produce unbounded stresses as $z \to \infty$ should be dropped from Eqs. (48)–(50) and (77)–(79) before imposing the end conditions. With this in mind, it is appropriate to define the characteristic decay length

$$L = \frac{\ln 100}{\kappa\lambda_n}, \tag{90}$$

as a simple measure to estimate the stress disturbance from the end in a long circular bar, which is the distance measured from the end beyond which the series terms contribute only 1% in magnitude to the deformation and stresses. In other words, the deformation and stresses in the region beyond L from the end are essentially independent of the load distribution over the end surface so that the Saint-Venant solution should be applicable. Of course, other percentage could be chosen for the estimation and the smallest eigenvalue λ_1 should be used to determine the largest L.

Knowing $\lambda_1 b = 5.1356$ for a homogeneous bar, so

$$L = \frac{\ln 100}{\kappa\lambda_1} = 0.8967b\sqrt{\frac{c_{44}}{c_{66}}}, \tag{91}$$

which suggests that the end effect is far-reaching for strong anisotropy ($c_{44} \gg c_{66}$). Since $c_{44} = c_{66}$ for isotropic materials, $L = 0.8967b$, suggesting that the stress disturbance is indeed confined to a local region near the end in a long homogeneous isotropic bar. Tables 1 and 2 show the smallest eigenvalue λ_1 associated with the parameter of the radial inhomogeneity μ, and the characteristic decay length L of long circular bars in connection with μ and the material parameter $\kappa = \sqrt{c_{66}/c_{44}}$. To show the effect of anisotropy, we take $c_{44}/c_{66} = 1, 4, 16, 100$ for computation. All cases are admissible in that they satisfy the requirement of positive-definiteness of the strain energy. Although $c_{44}/c_{66} = 100$ appears to be uncommon in practice, the value is as-

Table 1
The smallest eigenvalue for various inhomogeneity parameters

μ	0	0.1	0.2	0.5	1.0	2.0	3.0
$\lambda_1 b$	5.1356	5.2622	5.3883	5.7635	6.3802	7.5883	8.7715

Table 2
Characteristic decay length of long circular bars

L	Isotropic	$c_{44}=4c_{66}$	$c_{44}=16c_{66}$	$c_{44}=100c_{66}$
$\mu=0$	$0.897b$	$1.794b$	$3.587b$	$8.967b$
$\mu=0.5$	$0.799b$	$1.598b$	$3.196b$	$7.991b$
$\mu=1.0$	$0.722b$	$1.447b$	$2.887b$	$7.218b$

sumed in the interest of demonstrating the effect of strong anisotropy. Notably, the characteristic decay length could reach as far as $9b$ from the free end of a strongly orthotropic ($c_{44}=100c_{66}$) circular bar, not to the expectation based on Saint-Venant's conjuncture.

To examine quantitatively the Saint-Venant conjecture, we consider two types of torsional load prescribed over the end surface. Load type 1: linearly distributed load, $p(r)=qr$. Load type 2: tangential ring load applied at the boundary of the circular section, $p(r)=0.25qb^2\delta(r-b)$, where $\delta(r-b)$ is the Dirac-delta function. Both loading types give rise to a pure torque of the same magnitude. While the linearly distributed load is continuous over the end surface, the tangential ring load is concentrated at $r=b$. The influence of the radial inhomogeneity and material anisotropy are studied by taking the material parameters: $\mu=0$ (homogeneous material), $\mu=0.5$ (linearly distributed radial inhomogeneity) and $\mu=1.0$ (quadratically distributed radial inhomogeneity); $\kappa=1$ ($c_{44}=c_{66}$, isotropic material), $\kappa=0.5;0.25;0.1$ (orthotropic materials with $c_{44}=4c_{66}$; $c_{44}=16c_{66}$; $c_{44}=100c_{66}$, respectively) in the computation. In all the figures presented in the following the displacement and stresses have been made dimensionless.

Fig. 1 shows the variations of u_θ, $\sigma_{\theta z}$, and $\sigma_{r\theta}$ at $r=0.5b$ in the axial direction for cylindrically orthotropic, homogeneous bars ($\mu=0$) subjected to the tangential ring load (load type 2). When a homogeneous bar is subjected to linearly distributed load (load type 1), the deformation and stress distribution are identical to those of Saint-Venant's torsion. It can be observed that the end effect is far-reaching in circular bars with strong cylindrical orthotropy ($c_{44}=16c_{66}$; $c_{44}=100c_{66}$), whereas the stress disturbance in an isotropic bar

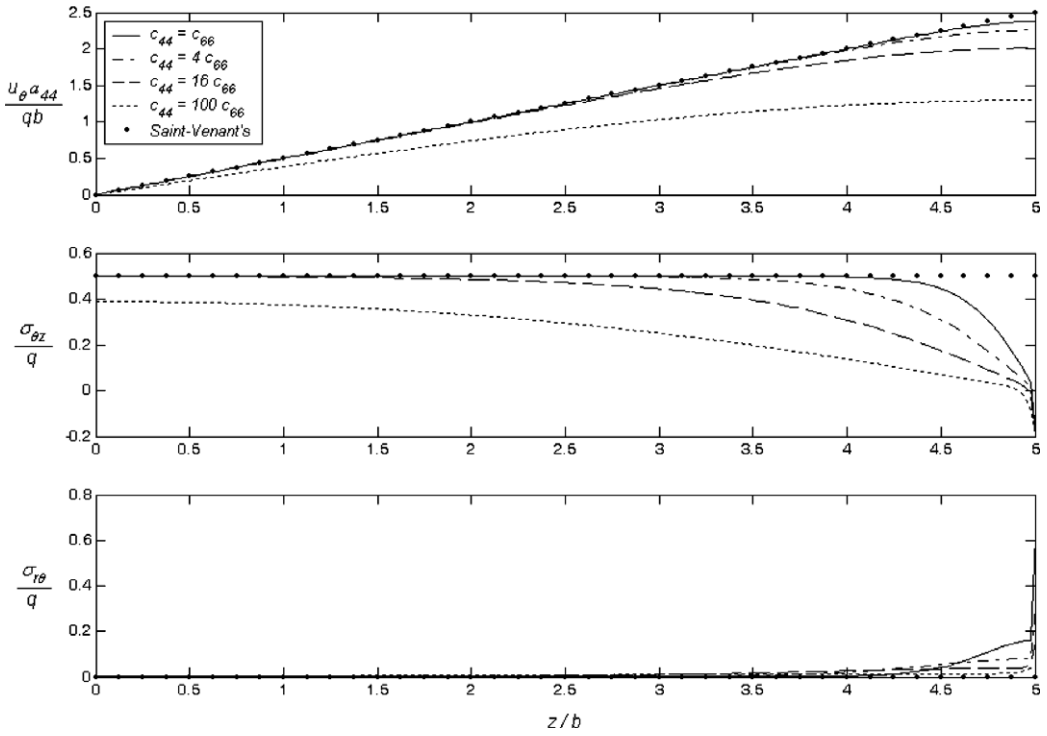

Fig. 1. Axial distribution of u_θ, $\sigma_{\theta z}$ and $\sigma_{r\theta}$ at $r=0.5b$ in homogeneous bars under tangential ring load (load type 2).

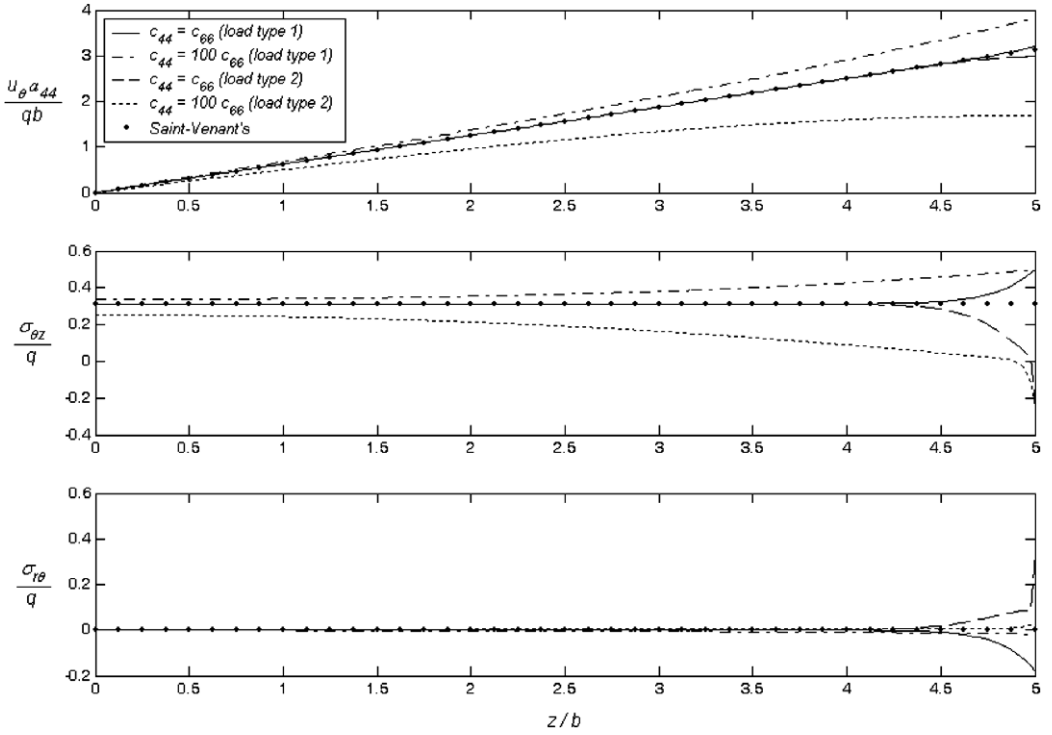

Fig. 2. Axial distribution of u_0, $\sigma_{\theta z}$ and $\sigma_{r\theta}$ at $r = 0.5b$ in non-homogeneous bars ($\mu = 0.5$) under linearly distributed load (load type 1) and tangential ring load (load type 2).

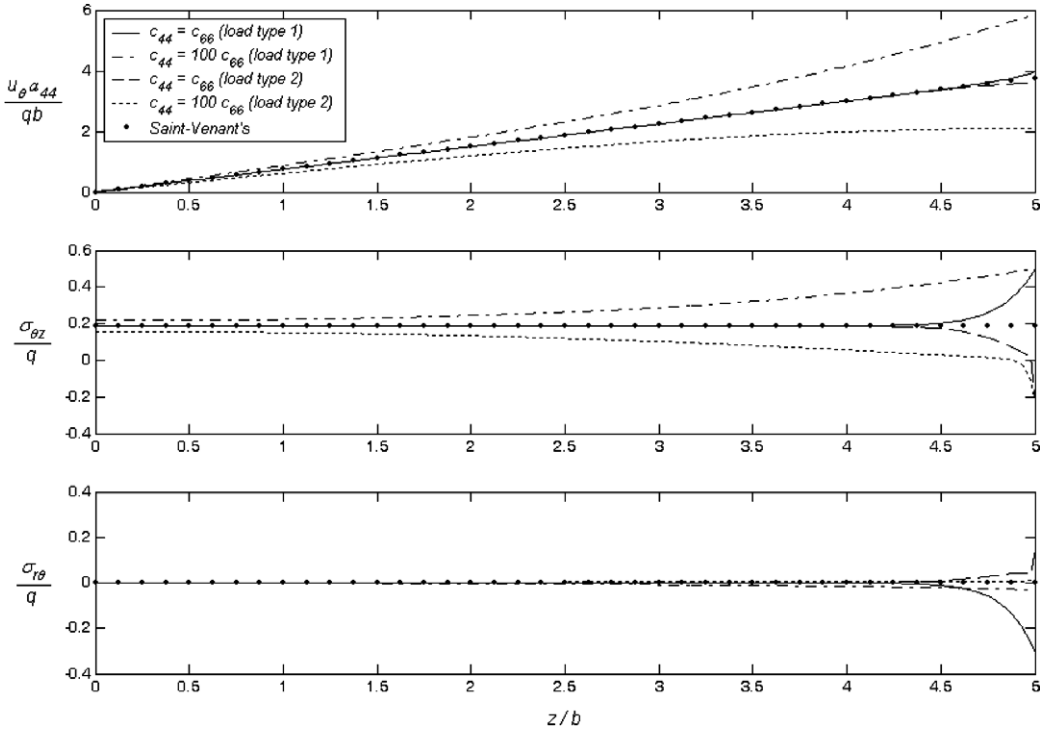

Fig. 3. Axial distribution of u_0, $\sigma_{\theta z}$ and $\sigma_{r\theta}$ at $r = 0.5b$ in non-homogeneous bars ($\mu = 1.0$) under linearly distributed load (load type 1) and tangential ring load (load type 2).

is confined to a local region near the free end. While the deviations of u_θ and $\sigma_{\theta z}$ from their Saint-Venant counterparts are remarkable, the end effect on $\sigma_{r\theta}$ is localized to the vicinity of the free end where the tangential ring load is acting.

Figs. 2 and 3 display the effects of radial inhomogeneity and prescribed torsion loads on the displacement and stress distribution at $r = 0.5b$ along the z axis in circular bars with radial inhomogeneity $\mu = 0.5$ and $\mu = 1.0$, in which the material is assumed to be isotropic ($c_{44} = c_{66}$) and strongly orthotropic ($c_{44} = 100c_{66}$), respectively. Both loading types exhibit end effects. The effect is far-reaching in the bar with strong anisotropy subjected to the tangential ring load. The radial inhomogeneity plays a less important role in the stress disturbance in view that the deviations from the Saint-Venant counterparts in the case of isotropy are confined to the region of a diameter from the free end for both cases of $\mu = 0.5$ and $\mu = 1.0$ for the reason that the characteristic decay length depends upon the smallest eigenvalue λ_1 which varies slightly for different μ, as given in Table 2.

Figs. 4–7 show the radial variations of the displacement and stresses at the sections $z = 0$ and $z = 4b$ in the bars subjected to two types of torsion load with material orthotropy and radial inhomogeneity. The section $z = 0$ is the fixed end; the section $z = 4b$ is chosen because it is generally expected that stress disturbance occurs within a diameter from the end according to the conjecture of Saint-Venant's torsion. The results show that at the fixed end Saint-Venant's solutions are in good agreement with the exact solution, except for a slight difference in $\sigma_{\theta z}$ in the case of strong orthotropy under tangential ring load (Fig. 7). Surprisingly, the non-vanishing stress $\sigma_{\theta z}$ at the fixed end does not vary significantly compared with that at $z = 4b$, which can be attributed to the fact that the fixed end is subjected to the same resultant torque as any other section of the circular bar under torsion; the prescribed BC affects only the stress distribution across the section. As for the displacement and stresses at the section $z = 4b$, Fig. 4 reveals that the stress disturbance is confined to the vicinity near the end where the torsion load is applied; small deviation from the exact solution is observed only in $\sigma_{r\theta}$. Thus Saint-Venant's conjecture is applicable to torsion of isotropic circular bars even with radial inhomogeneity. In the case of anisotropic materials the situation is different in view of Figs. 5–7. The stresses are greatly disturbed by the traction BC at $z = 5b$. As shown in Figs. 6,7, the end effect is sig-

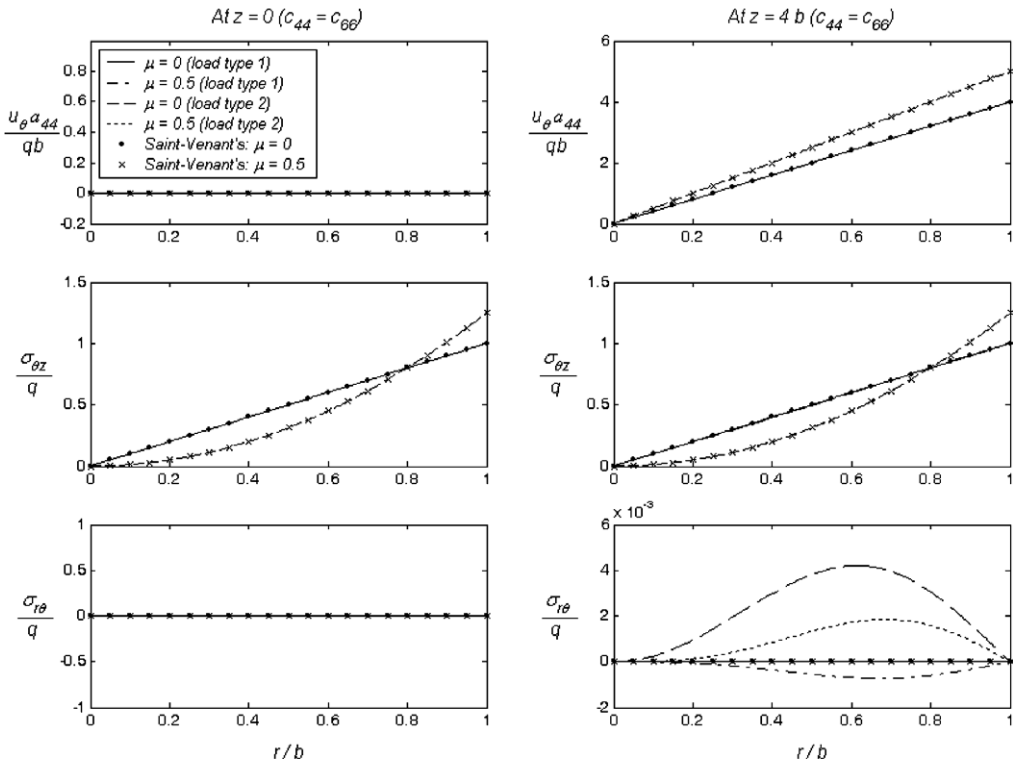

Fig. 4. Radial distribution of u_θ, $\sigma_{\theta z}$ and $\sigma_{r\theta}$ at $z = 0$; $4b$ in isotropic bars under linearly distributed load (load type 1) and tangential ring load (load type 2).

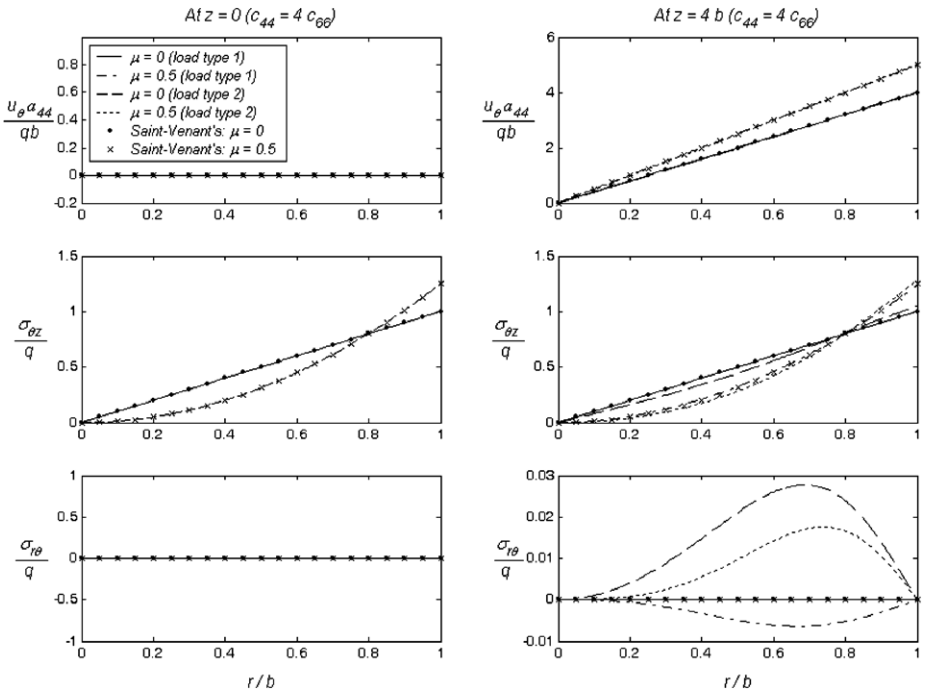

Fig. 5. Radial distribution of u_θ, $\sigma_{\theta z}$ and $\sigma_{r\theta}$ at $z = 0$; $4b$ in orthotropic bars ($c_{44} = 4c_{66}$) under linearly distributed load (load type 1) and tangential ring load (load type 2).

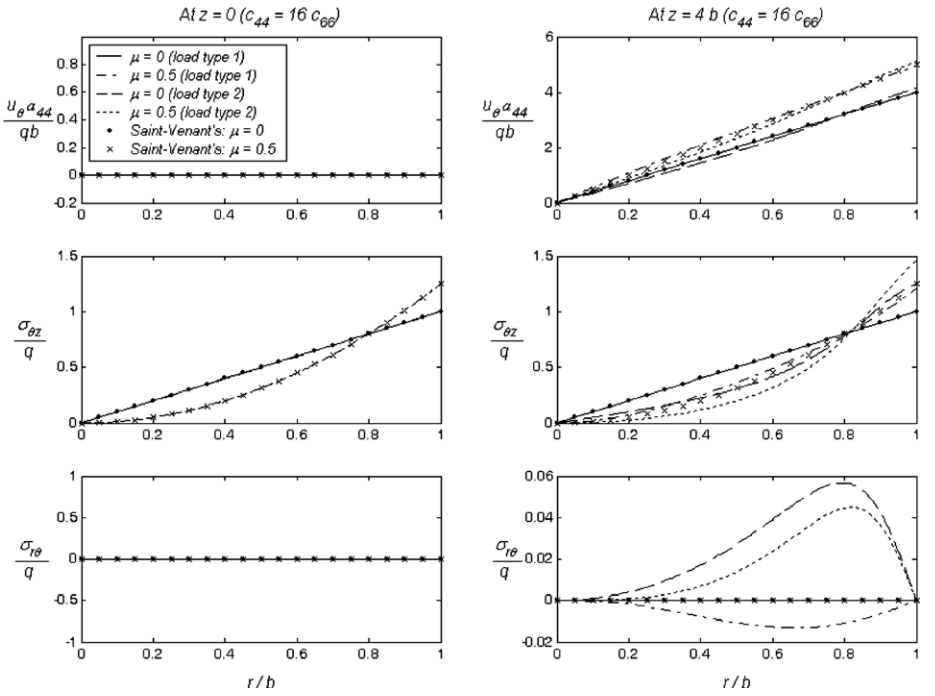

Fig. 6. Radial distribution of u_θ, $\sigma_{\theta z}$ and $\sigma_{r\theta}$ at $z = 0$; $4b$ in orthotropic bars ($c_{44} = 16c_{66}$) under linearly distributed load (load type 1) and tangential ring load (load type 2).

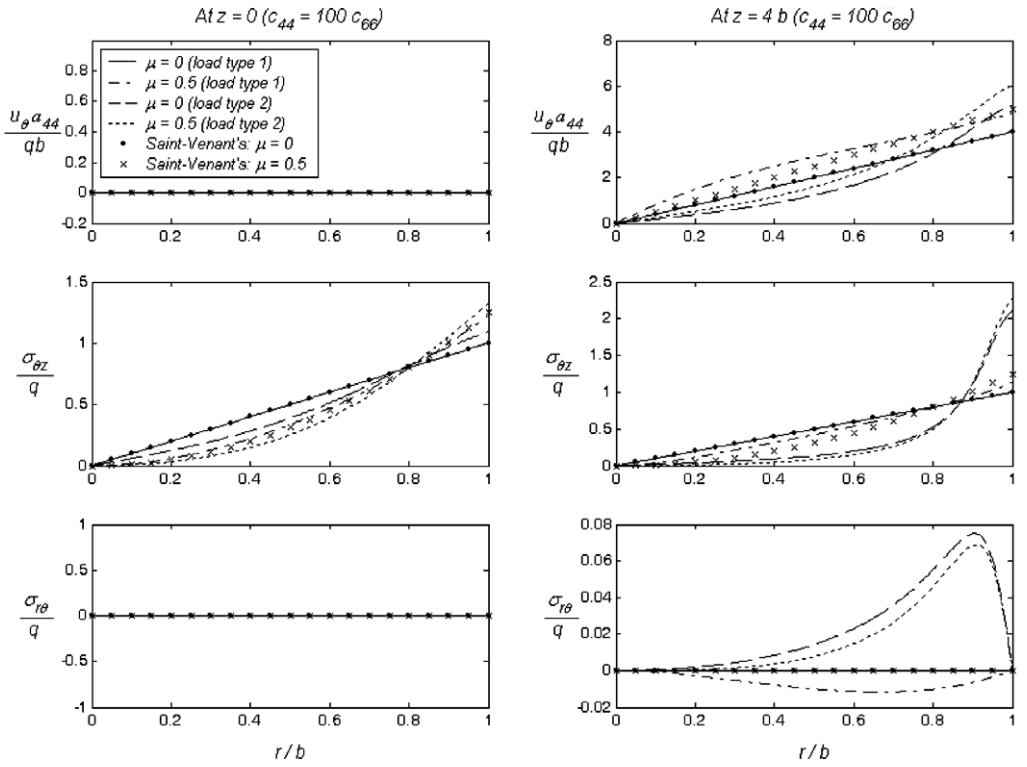

Fig. 7. Radial distribution of u_θ, $\sigma_{\theta z}$ and $\sigma_{r\theta}$ at $z = 0$; $4b$ in orthotropic bars ($c_{44} = 100c_{66}$) under linearly distributed load (load type 1) and tangential ring load (load type 2).

nificant in finite circular bars with strong orthotropy subjected to tangential ring load. Remarkable differences exist between the exact solution and the Saint-Venant solution in which the exact traction BC are relaxed by the statically equivalent ones.

6. Conclusions

The present study enables us to assess Saint-Venant's principle as applied to anisotropic, non-homogeneous elastic bodies in general and to evaluate the stress diffusion in torsion of radially inhomogeneous, cylindrically orthotropic cylinders in particular. The following conclusions can be drawn from the analysis.

(1) The classical solution based on the Saint-Venant conjecture is useful for torsion of isotropic circular bars with or without radial inhomogeneity. The stress disturbance is confined to the local region near the end where the torsion load is applied.
(2) The stresses at the fixed end of circular bars under torsion can be evaluated using the solution based on Saint-Venant's conjecture except in the case of strong anisotropy.
(3) Radial inhomogeneity of the material affects the deformation and stress distribution in cylindrically orthotropic bars, but it is not significant in evaluating the stress disturbance due to the end effect.
(4) The end effect is far-reaching and cannot be ignored in torsion of circular bars with strong anisotropy. The Saint-Venant conjecture should be used with caution in such cases.

Acknowledgement

The work is supported by the National Science Council of Taiwan, ROC through Grant NSC 95-2211-E006-468.

References

Chen, T., Wei, C.J., 2005. Saint-Venant torsion of anisotropic shafts: theoretical framework, extremal bounds and affine transformations. Quarterly Journal of Mechanics and Applied Mathematics 58, 269–287.

Christensen, R.M., 1994. Properties of carbon fibers. Journal of the Mechanics and Physics of Solids 42, 681–695.

Dong, S.B., Kosmatka, J.B., Lin, H.C., 2001. On Saint-Venant's problem for an inhomogeneous, anisotropic cylinder. Part I: Methodology for Saint-Venant's solutions. Journal of Applied Mechanics 68, 376–381.

Folkes, M.J., Arridge, R.G.C., 1975. The measurement of shear modulus in highly anisotropic materials: the validity of St Venant's principle. Journal of Physics D: Applied Physics 8, 1053–1064.

Hildebrand, F.B., 1976. Advanced Calculus for Applications, 2nd ed. Prentice-Hall, Englewood Cliffs, New Jersey.

Horgan, C.O., 1972. Some remarks on Saint-Venant's principle for transversely isotropic composites. Journal of Elasticity 2, 335–339.

Horgan, C.O., 1982. Saint-Venant end effects in composites. Journal of Composite Materials 16, 411–422.

Horgan, C.O., 1989. Recent developments concerning Saint-Venant's principle: an update. Applied Mechanics Reviews 42, 295–303.

Horgan, C.O., 1996. Recent developments concerning Saint-Venant's principle: a second update. Applied Mechanics Reviews 49, S101–S111.

Horgan, C.O., Carlsson, L.A., 2000. Saint-Venant end effects for anisotropic materials. In: Kelly, A., Zweben, C. (Eds.), Comprehensive Composite Materials, vol. 5. Elsevier, Oxford, pp. 5–21.

Horgan, C.O., Chan, A.M., 1999. Torsion of functionally graded isotropic linearly elastic bars. Journal of Elasticity 52, 181–199.

Horgan, C.O., Miller, K.L., 1995. Saint-Venant end effects for plane deformations of elastic composites. Mechanics of Composite Materials and Structures 2, 203–214.

Horgan, C.O., Simmonds, J.G., 1994. Saint-Venant end effects in composite structures. Composites Engineering 4, 279–286.

Huang, C.H., Dong, S.B., 2001. Analysis of laminated circular cylinders of materials with the most general form of cylindrical anisotropy, Part I: Axially symmetric deformations. International Journal of Solids and Structures 38, 6163–6182.

Kosmatka, J.B., Lin, H.C., Dong, S.B., 2001. On Saint-Venant's problem for an inhomogeneous, anisotropic cylinder. Part II: Cross-sectional properties. Journal of Applied Mechanics 68, 382–391.

Lekhnitskii, S.G., 1981. Theory of Elasticity of an Anisotropic Body. Mir, Moscow.

Lin, H.C., Dong, S.B., Kosmatka, J.B., 2001. On Saint-Venant's problem for an inhomogeneous, anisotropic cylinder. Part III: End effects. Journal of Applied Mechanics 68, 392–398.

Rooney, F.J., Ferrari, M., 1995. Torsion and flexure of inhomogeneous elements. Composite Engineering 5, 901–911.

Scalpato, M.R., Horgan, C.O., 1997. Saint-Venant decay rates for an isotropic inhomogeneous linearly elastic solid in anti-plane shear. Journal of Elasticity 48, 145–166.

Sokolnikoff, I.S., 1956. Mathematical Theory of Elasticity. McGraw-Hill, New York.

Tarn, J.Q., 2001. Exact solutions for functionally graded anisotropic cylinders subjected to thermal and mechanical loads. International Journal of Solids and Structures 38, 8189–8206.

Tarn, J.Q., 2002a. Exact solutions of a piezoelectric circular tube or bar under extension, torsion, pressuring, shearing, uniform electric loadings and temperature change. Proceedings of the Royal Society of London A 458, 2349–2367.

Tarn, J.Q., 2002b. A state space formalism for anisotropic elasticity. Part II: Cylindrical anisotropy. International Journal of Solids and Structures 39, 5157–5172.

Tarn, J.Q., Chang, H.H., 2005. Extension, torsion, bending, pressuring and shearing of piezoelectric circular cylinders with radial inhomogeneity. Journal of Intelligent Material Systems and Structures 16, 631–641.

Tarn, J.Q., Wang, Y.M., 2001. Laminated composite tubes under extension, torsion, bending, shearing and pressuring: a state space approach. International Journal of Solids and Structures 38, 9053–9075.

Ting, T.C.T., 1999. New solutions to pressuring, shearing, torsion, and extension of a cylindrically anisotropic elastic circular tube or bar. Proceedings of the Royal Society of London A 455, 3527–3542.

Watson, G.N., 1995. A Treatise on the Theory of Bessel Functions. Cambridge University Press, Cambridge, Cambridge mathematical Library edition.

Yang, Y.Y., 2000. Time-dependent stress analysis in functionally graded materials. International Journal of Solids and Structures 37, 7593–7608.